Effect of ZnO Nanostructure Morphology on the Sensing of H2S Gas

ARTICLE *in* THE JOURNAL OF PHYSICAL CHEMISTRY C · NOVEMBER 2013

Impact Factor: 4.77 · DOI: 10.1021/jp408916b

2 AUTHORS:

Kalon Jake Iversen
La Trobe University
10 PUBLICATIONS **69** CITATIONS
SEE PROFILE

Michelle J S Spencer
RMIT University
59 PUBLICATIONS **665** CITATIONS
SEE PROFILE

THE JOURNAL OF PHYSICAL CHEMISTRY C

Article

pubs.acs.org/JPCC

Effect of ZnO Nanostructure Morphology on the Sensing of H_2S Gas

Kalon J. Iversen[†] and Michelle J. S. Spencer*[,†,‡]

[†]Department of Chemistry, La Trobe Institute for Molecular Science, La Trobe University, Melbourne, Victoria 3086, Australia

[‡]School of Applied Sciences, RMIT University, GPO Box 2476, Melbourne Victoria 3001, Australia

ABSTRACT: Detection of pollutant gases, such as H_2S, is of high importance for health reasons. We examine the effect of ZnO nanostructure morphology on the sensing mechanism of H_2S, using density functional theory calculations. The effect of nanostructure size and shape, gas coverage, and reaction temperature are analyzed in order to determine the effect that each has on the gas−surface reaction. We show that H_2S dissociatively chemisorbs on the nanowire and faceted-nanotube as H and SH, while H_2S molecularly physisorbs on the nanotube. H_2S can adsorb in multiple locations and orientations on the nanowire and faceted-nanotube with the faceted-nanotube providing a greater number of surface sites due to its larger outer surface area and the fact that H_2S can also adsorb on the inside of the structure. H_2S acts as a charge donor, causing a decrease in the band gap after adsorption on the nanowire and faceted-nanotube, while the band gap for the nanotube remained almost unchanged after H_2S adsorption. Using ab initio molecular dynamics simulations, we show that H_2S may poison the nanowire and faceted-nanotube surface, while H_2S causes the nanotube structure to distort significantly.

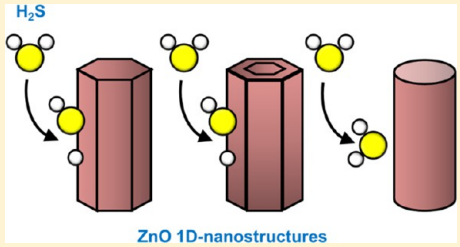

1. INTRODUCTION

The detection of dangerous gases is an important factor for the safety of people and the environment. Hydrogen sulfide (H_2S) is a colorless gas with the distinct smell of rotten eggs and is readily produced as a byproduct in at least 70 industries ranging from petroleum refining, farming and waste management (i.e., landfill), to natural gas production.[1,2] The toxic effects of H_2S were first documented roughly 300 years ago; it is extremely dangerous due to its flammability as well as its high lipid solubility, which allows it to pass through the cellular membranes in the body, preventing cellular respiration.[1] It also has the ability to paralyze the sense of smell at higher concentrations (100 ppm), which prevents it from being recognized, with the concentration becoming lethal at 500 ppm.[1,2] These factors, combined with its increasing prevalence in the atmosphere[3] make it necessary to develop low cost and more efficient sensing devices capable of detecting the gas.

Metal oxides have been used as sensors for many decades to detect a variety of toxic and harmful gases. Traditionally, these sensing devices consist of a thin film of an oxide material, and operate by measuring a change in conductivity after a gas adsorbs on the surface. With the recent discovery of novel nanostructured forms of ZnO, in particular, their application in sensing devices has been investigated, showing they often have a better sensing response than the thin film sensor.[4] One major focus for gas sensing has been the one-dimensional (1D) form, which includes nanorods (or nanowires) and faceted nanotubes, which have side facets commonly consisting of the wurtzite $\{10\bar{1}0\}$ surface. It should be noted that the difference between a ZnO nanorod and a nanowire is that nanorods have a hexagonal cross section, while nanowires may not.

Cao et al.,[5] Wang et al.,[6] and Kim et al.[7] investigated the use of ZnO nanorods for monitoring H_2S gas, showing an improved ability to detect H_2S over other gases, with Cao et al.[5] and Wang et al.[6] finding an increased response and selectivity through the use of ZnO nanorods over bulk ZnO. They also described a quick response time to low concentrations of H_2S, with detection as low as 0.05 ppm measurable at room temperature.[6] Kim et al.[7] found a similar response and selectivity with an exponential increase in response to H_2S at temperatures above 300 °C. Both studies also measured an increase in conductivity when H_2S adsorbed on the ZnO nanorod surface, which they attributed to H_2S interacting and decreasing the concentration of preadsorbed oxygen.[6,7] While ZnO nanorods were investigated in these studies, other morphologies, such as ZnO faceted nanotubes and nanotubes are yet to be analyzed. Furthermore, the reactions occurring on the nanorod surface after adsorption of H_2S are still not completely understood.

The sensing mechanism of these resistance-type metal oxide sensors is usually described by the surface-depletion model. During the sensing process, H_2S can interact, or adsorb directly on the oxide surface, or with preadsorbed oxygen that is present on the surface. When the gas adsorbs it can alter the thickness of the depletion layer, causing a change in the measured resistivity. For H_2S, which is a reducing gas, it causes a decrease in measured resistivity by releasing electrons back into the conduction band and reducing the thickness of the depletion layer. In this study we focus on the interaction of H_2S directly with the clean ZnO surface.

The theoretical studies to date have focused on the reaction of H_2S with the bulk-terminated $(10\bar{1}0)$ surface, including the density functional theory (DFT) calculations of Casarin et al.,[8] Ling et al.[9] and Goclon and Meyer.[10] The effect of ZnO

Received: September 5, 2013
Revised: November 7, 2013
Published: November 8, 2013

   dx.doi.org/10.1021/jp408916b | J. Phys. Chem. C 2013, 117, 26106−26118

nanostructure morphology, and in particular the effect of edges or surface curvature, on the reaction with H_2S, however, has not yet been determined. Such information is necessary to assist in the development of ZnO nanostructure based gas sensors.

In this work we use DFT calculations to compare the adsorption of H_2S on three different 1D ZnO nanostructures: a hexagonal nanowire, a faceted-nanotube, and a zigzag (9,0) nanotube. The effects of nanostructure size and shape, gas coverage as well as temperature on the gas-sensor reaction are determined in order to better understand the sensing mechanism. This work provides new insights into the effect of ZnO nanostructure morphology on the sensing of H_2S, which is important for the further development of nanostructure-based sensor devices.

2. METHOD

2.1. Computational Methodology. All of the calculations in this study were performed using density functional theory as implemented in the Vienna Ab initio Simulation Package (VASP).[11−13] The plane wave pseudopotential approach was used with a 400 eV cutoff energy and a generalized gradient approximation (GGA) with the Perdew and Wang functional (PW91).[14] Vanderbilt ultrasoft pseudopotentials (USPPs) as supplied in VASP[15] were implemented. A Monkhorst and Pack k-point mesh of 1 × 1 × 8 was used to perform k-point sampling.[16]

2.2. Nanostructure Models. The nanowire, faceted-nanotube and (9,0) zigzag nanotube calculations were performed using a supercell model with periodic boundary conditions (PBCs). The nanostructures were cleaved from a bulk wurtzite ZnO structure with lattice constants of a = 3.268 Å and c = 5.233 Å and internal parameter of u = 0.3826 (as determined previously[17]).

Each nanostructure was initially constructed by cleaving rings of different sizes from the bulk ZnO structure. As PBCs are used, each cleaved structure has a vacuum spacer of at least 12 Å in the x- and y- directions to avoid interaction between nanostructures in adjacent cells. Replication of the cell in the z-direction reproduces the length of each nanostructure.

The three nanostructures were optimized by allowing all atoms in the structure to relax while changing the length of the supercell in the z-direction until the total energy had converged to 10^{-4} eV, and the Hellmann−Feynman force on each atom was less than 0.02 eV/Å. The minimum energy structure for the nanowire, faceted-nanotube, and nanotube were found to have z-lengths of 5.403 Å, 5.413 Å and 5.653 Å, respectively. The diameter of each of each nanostructure was 9.81 Å (nanotube; measured as d(O−O) or 9.31 Å from d(Zn−Zn), 16.59 Å (faceted-nanotube; measured as d(O−O) or 16.05 Å from d(Zn−Zn) and 9.54 Å (nanotube). The nanowire contains 24 Zn and 24 O atoms, the faceted-nanotube 48 Zn and 48 O atoms, and the nanotube 18 Zn and 18 O atoms. The optimized geometry of each nanostructure is shown in Figure 1. The nanowire has the same hexagonal cross section as that of the nanorods that have been studied experimentally for H_2S detection.[5−7] The faceted nanotube also has a hexagonal cross section, however, is hollow in the middle. The nanotube, in contrast, has a cylindrical cross section (after optimization) as shown in Figure 1.

To model the adsorption of H_2S, the adsorbate was initially positioned ∼3 Å from the surface above different adsorption sites, including atop zinc, atop oxygen, bridge, and hollow sites. Different initial orientations of H_2S were also tested for each

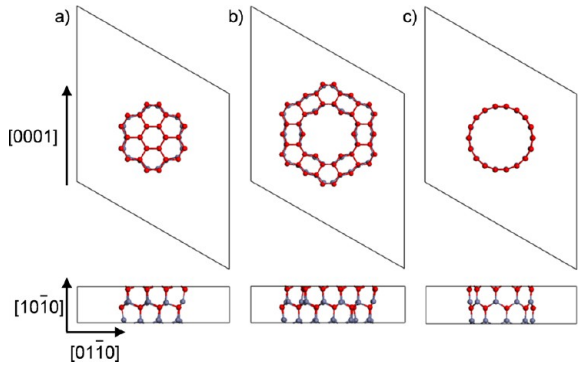

Figure 1. One-dimensional ZnO (a) nanowire, (b) faceted-nanotube, and (c) nanotube, cleaved from the bulk ZnO. Top view (top) and side view (bottom) of each nanostructure.

site, with either the H or S atoms pointing towards the adsorption site. It was noted that after geometry optimization, the adsorbates did not always remain in the initial adsorption site. Three adsorption coverages were examined by placing 1, 3, or 6 H_2S molecules on each nanostructure. For the faceted-nanotube and nanotube, adsorption of H_2S on the inside of the nanostructure was also considered. Calculations were performed as spin-polarized.

The binding energy (BE) values of H_2S adsorbed on each nanostructure were calculated using the following formula:

$$\mathrm{BE} = \frac{[E_{(\mathrm{ads/ZnO})} - (nE_{\mathrm{ads}} + E_{\mathrm{ZnO}})]}{n} \quad (1)$$

where $E_{(\mathrm{ads/ZnO})}$ is the total energy of the H_2S/nanostructure system, E_{ads} is the total energy of the H_2S molecule, E_{ZnO} is the total energy of the clean ZnO nanostructure, with n representing 1, 3, or 6 H_2S molecules. Using eq 1, the stable structures have negative binding energies, while unstable structures have positive binding energies. The H_2S molecule was optimized in a 15 × 15 × 15 Å^3 sized cell with an optimized S−H bond length of 1.35 Å and bond angle of 91.6°, which closely match the experimental values of 1.336 Å and 92.1°,[18] respectively.

Vibrational frequency calculations were performed by diagonalizing a finite difference construction of the Hessian matrix with displacements of 0.015 Å (allowing only the adsorbate atoms to move). An attempt was made to only include minimum-energy structures with all real vibrational frequencies, however, due to vibrational frequency calculations being highly computationally demanding not all structures were analyzed. It is important to note that the most stable structures calculated were confirmed to be minima.

The Bader charges on individual atoms were calculated according to the procedure described by Henkelman et al.[19] In order to test whether this procedure was appropriate for these calculations using USPPs, we performed sample calculations using the projector augmented wave (PAW) functionals.[20] We found that the values only changed by <0.03 e even after geometry optimization was performed. However, for the USPPs more dense FFT grids (2x) were necessary to obtain converged results.

The ab initio MD calculations were performed using the VASP code. The simulations were run at 300 K and/or 700 K, using a time step of 0.5 fs. A Verlet algorithm was used to integrate the equations of motion, with the temperature being controlled by the Nosé thermostat.[21] The simulations were

dx.doi.org/10.1021/jp408916b | J. Phys. Chem. C 2013, 117, 26106−26118

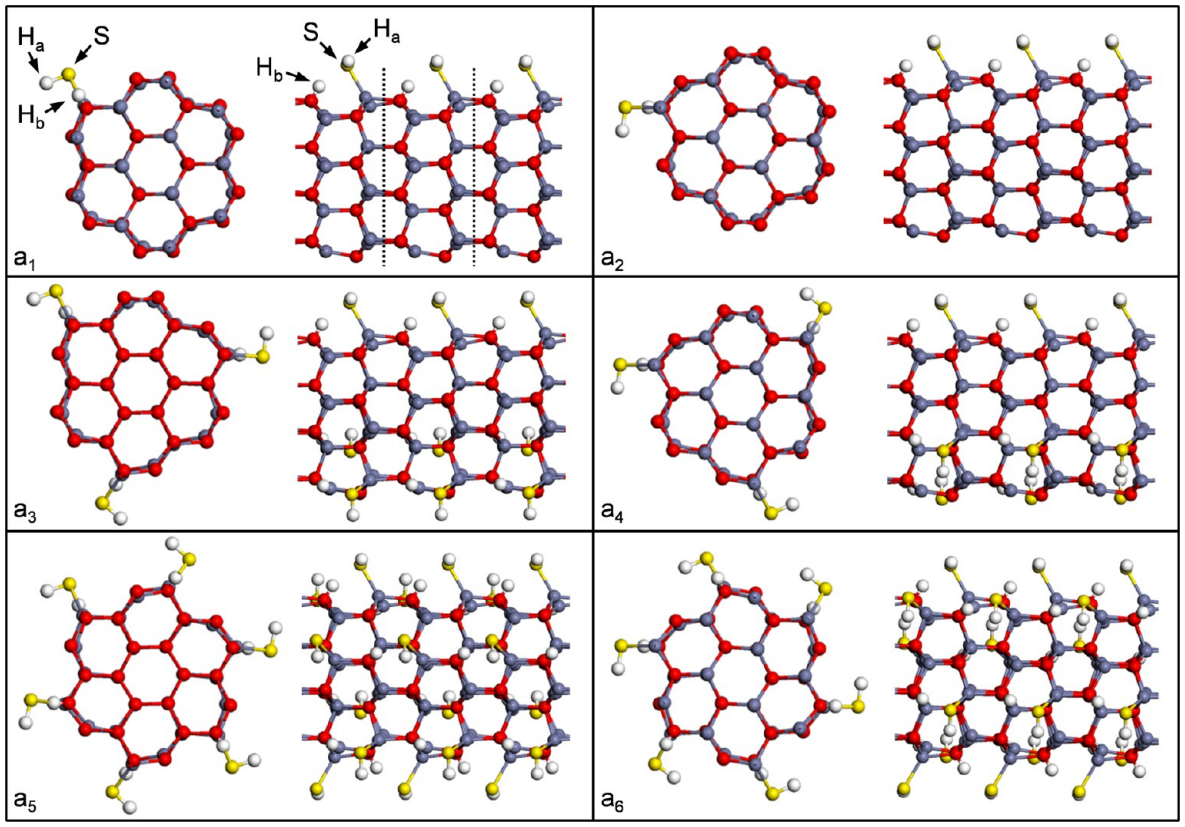

Figure 2. ZnO nanowire with one ($a_{1,2}$), three ($a_{3,4}$), or six ($a_{5,6}$) H_2S molecules adsorbed. The supercell boundary along the *z*-direction is indicated by the black dashed line (shown for a_1 only).

Table 1. Calculated Properties of H_2S Adsorbed on the ZnO Nanowire at the Coverages Indicated

#H_2S	structure	E_B (eV)	$d(Zn_S–SH_a)$ (Å)	$d(S–H_a)$ (Å)	$d(O_S–H_b)$ (Å)	$\angle Zn_SSH_a$ (°)	$\nu(S–H_a)$(cm^{-1})	$\nu(O_S–H_b)$ (cm^{-1})	E_g (eV)	Δq (e)
--	H_2S	--	--	1.35	--	--	2627[a]	3657[b]	--	--
--	ZnO	--	--	--	--	--	--	--	1.57	--
1	a_1	−1.26	2.28	1.35	1.02	94	2612	2885	1.27	0.12
	a_2	−1.26	2.28	1.35	1.02	97	2614	2883	1.27	0.12
3	a_3	−1.25	2.28 × 3	1.35 × 3	1.02 × 3	94 × 3	2615 × 3	2871 × 3	1.31	0.36
	a_4	−1.25	2.28 × 3	1.35 × 3	1.02 × 3	97 × 3	2613 × 3	2868 × 3	1.31	0.37
6	a_5	−1.30	2.27 × 6	1.35 × 6	1.01 × 6	94 × 6	2613 × 6	2903 × 6	1.45	0.78
	a_6	−1.30	2.27 × 6	1.35 × 6	1.02 × 6	97 × 6	2612 × 6	2991	1.45	0.77
								2844 × 5		

Binding energy (E_B); calculated distance between the Zn_S and S of SH ($d(Zn_S–SH_a)$); SH distance ($d(S–H_a)$); O_S surface atom and H distance ($d(O_S–H_b)$); bond angle between the Zn_S and SH ($\angle(Zn_SSH)$); calculated S–H stretch ($\nu(S–H_a)$) and O–H stretch ($\nu(O_S–H_b)$); band gap (E_g); charge transfer (Δq); [a]Calculated symmetric stretch of H_2S molecule. [b]Symmetric stretch of H_2O.[18]

performed by either starting with H_2S positioned ∼3 Å from the surface above different adsorption sites, or from the optimized structure obtained after geometry optimization. These simulations were run for up to 12 ps, during which time all atoms were allowed to relax.

3. RESULTS AND DISCUSSION

3.1. H_2S/ZnO Nanowire. *3.1.1. Binding Energy and Geometry.* From the calculations it was determined that there are two stable structures of adsorbed H_2S at each coverage analyzed (see Figure 2). The associated parameters calculated for each structure are presented in Table 1. For all calculations it was found that the H_2S molecule dissociated on the nanowire (during geometry optimization) to form adsorbed H and SH, with the reaction being expressed as

$$H_2S_{(g)} \rightarrow H_{(ads)} + SH_{(ads)} \quad (2)$$

This suggests that there is little or no barrier to dissociation, which is the same as for the reaction of H_2S with the extended planar $(10\bar{1}0)$ surface.[10] In each case it was found that the H atom adsorbed to a surface O atom (O_s) and the SH species adsorbed to a surface Zn atom (Zn_s), via the S atom, which is the same as determined for H_2S adsorption on the $(10\bar{1}0)$ surface,[9,10,22] and which is the structure on the sides of the nanowire we examine here. The two structures found at each gas coverage were shown to differ in the orientation of the SH species relative to the nanostructure, with the H atom being positioned either away or toward the ZnO surface (Figure 2), corresponding to a Zn_SSH angle of either 94° or 97°. The bond lengths between the adsorbed H and SH and the corresponding nanostructure surface atoms were similar for the different gas

dx.doi.org/10.1021/jp408916b | J. Phys. Chem. C 2013, 117, 26106−26118

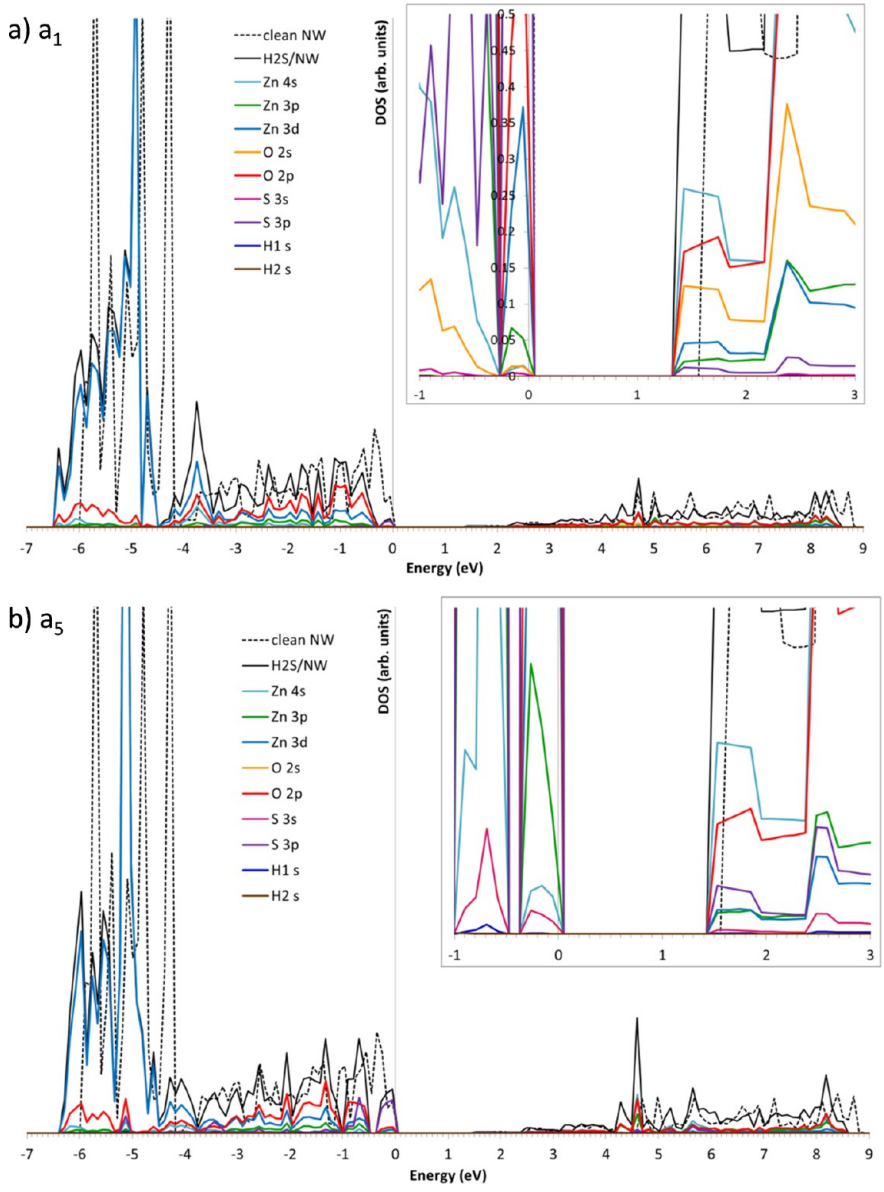

Figure 3. Density of states of H_2S adsorbed on the ZnO nanowire: (a) structure a_1 and (b) structure a_5. Inset shows magnified region of DOS around the band gap.

coverages (only varying by 0.01 Å), with a Zn_S-SH_a distance of ~2.28 Å and O_S-H_b distance of ~1.02 Å. These distances compare very closely to experimental values for the bond lengths in bulk ZnS (2.34 Å) and a water molecule (0.96 Å),[18] respectively, suggesting the formation of strong chemical bonds.

As shown in Table 1, the binding energies are the same for both structures at each gas coverage, with the magnitude of the values indicating that the H and SH are chemisorbed on the surface (consistent with the adsorbate−substrate bond lengths). As the gas coverage is increased, the BE values become slightly stronger (though the difference is ≤0.05 eV). This indicates that there is little interaction between adjacent adsorbed species, as this can weaken the interaction with the surface.

Both the geometry and BE calculated for the H_2S/nanowire structures are similar to those found by Casarin et al.,[8] for adsorption of H_2S on the ZnO(10$\bar{1}$0) surface, using a cluster approach; however, they calculated a stronger BE (−1.65 eV) and a slightly smaller interaction distance (2.22 Å). Similarly, for the more recent studies of H_2S/ZnO(10$\bar{1}$0) by Golcon and Meyer[10] and Ling et al.,[9] they also calculated stronger binding energy values of between −1.36 eV to −1.77 eV, and slightly longer Zn−S bond length of 2.32 Å.[9] While these differences may be partly attributed to the differences in computational approaches used, we suggest that adsorption of H_2S on ZnO nanowires is weaker than on the planar ZnO(10$\bar{1}$0) surface due to faceting of the surface and quantum size effects.

3.1.2. Vibrational Frequencies. The calculated vibrational frequencies for the most stable structures are shown in Table 4.1, with the values for the $S-H_a$ stretch and O_S-H_b stretch being presented. It can be seen that the $S-H_a$ stretch (~2610 cm^{-1}) for the dissociatively adsorbed H_2S has only decreased by ~15 cm^{-1} compared to the free molecule (2627 cm^{-1}), while the O_S-H_b stretch (~2900 cm^{-1}) has shifted by at least 750 cm^{-1} when compared to the O−H stretch of a free H_2O molecule (~3700 cm^{-1}). This large shift can be attributed to the surrounding environment of the O atom that is coordinated to three Zn atoms. Hence, experimentally, the presence of

dx.doi.org/10.1021/jp408916b | J. Phys. Chem. C 2013, 117, 26106−26118

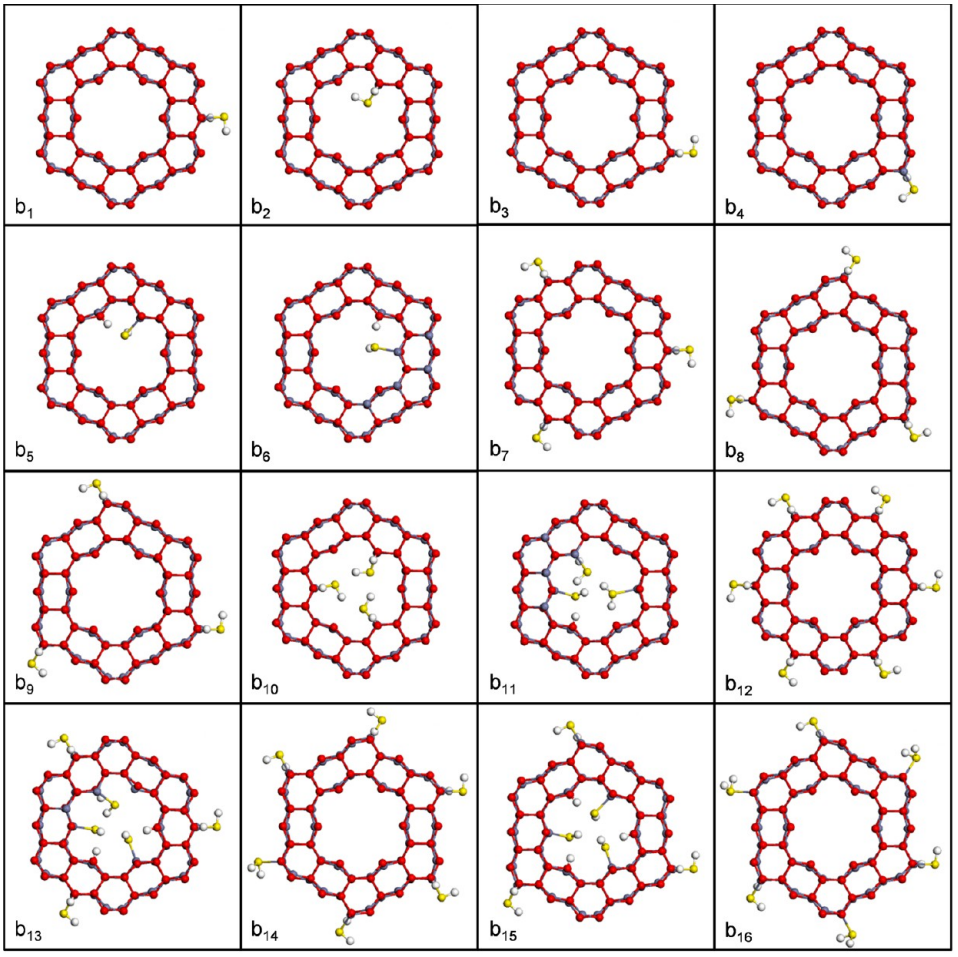

Figure 4. ZnO faceted-nanotube with one (b_{1-6}), three (b_{7-11}), or six (b_{13-16}) H_2S molecules adsorbed.

dissociatively adsorbed H_2S could be detected by the presence of an S−H and O−H stretch.

3.1.3. Charge Transfer, Band Structure and Density of States. The effect that different gases have on the electronic properties and conductance of a system underlies the gas sensing mechanism. Even though some DFT functionals underestimate the band gap of semiconductors, such calculations are useful for determining changes to the band gap after adsorption of a gas.

The calculated charge transfer (Δq) was determined to be positive for all six H_2S/nanowire structures (see Table 1). A positive Δq value indicates there is a transfer of charge from H_2S to the nanowire, and H_2S is acting as a charge donor. This is in contrast to other molecules, such as NO_2, NO, and N_2O, for example, that act as charge acceptors,[17,23−27] however, is consistent with the experimental results of, for example, Wang et al.[6] and Kim et al.[7] who detect an increase in conductivity when sensing H_2S using ZnO nanorods. A difference in this property for different gases allows one to distinguish between them, which is necessary for an effective gas sensor. We calculated that there is a linear correlation between increasing gas coverage and an increase in transfer of charge, which indicates that there would be a greater sensor response at higher gas coverages (i.e., increased gas concentration). The charge transfer per molecule is slightly larger for the highest coverage, which explains the slightly larger binding energy.

The partial density of states (PDOS), resolved to specific atoms and orbitals, for the H_2S/nanowire structure a_1 is shown in Figure 3a. The DOS are aligned so that the zero of energy is at the top of the valence band. For the clean nanowire, the main contribution to the states at the top of the valence band are primarily from the O 2p states followed by Zn 3d states, while the bottom of the conduction band is dominated by Zn 4s states, with smaller contributions from O 2p, followed by O 2s states. This is in good agreement with previous DFT calculations of this clean nanowire (see ref 28 and refs therein, for example).

After adsorption of H_2S, new states are introduced at −3.7 eV, −4.9 eV and between −6.0 to −6.5 eV. The H s-orbitals contribute to states deep within the valence band, at approximately −3.7 eV. From the magnified region (inset Figure 3a), it can be seen that impurity states from H_2S are also produced at the band edges. In particular, an impurity state is introduced below the bottom level of the conduction band, at approximately 1.3 eV. This new state is due to mixing of S 3p-orbitals with Zn 4s orbitals, O 2p, 2s orbitals as well as Zn 3d and 3p orbitals. At the top of the valence band, H_2S introduces some impurity states from mixing of S 3p-orbitals with surface Zn d-orbitals. It is important to note that it is this impurity state forming below the bottom level of the conduction band, which causes the decrease in the calculated band gap (see Table 1) and hence can be related to the change in electrical properties of the nanostructure.

For the most stable structures with three and six adsorbed H_2S molecules (structures a_3 and a_5), the PDOS show similar features with new impurity states located at the bottom of the

dx.doi.org/10.1021/jp408916b | J. Phys. Chem. C 2013, 117, 26106−26118

Table 2. Calculated Properties of H_2S Adsorbed on the ZnO Faceted-Nanotube at the Coverages Indicated

#H_2S	structure	E_B (eV)	$d(Zn_S\text{-}SH_a)$ (Å)	$d(S{-}H_a)$ (Å)	$d(O_S\text{-}H_b)$ (Å)	$\angle Zn_SSH_a$ (°)	$\nu(S{-}H_a)$ (cm^{-1})	$\nu(O_S\text{-}H_b)$ (cm^{-1})	E_g (eV)	Δq (e)
--	H_2S	--	--	1.35	--	--	2627[a]	3657[b]	--	--
--	ZnO	--	--	--	--	--	--	--	1.54	--
1	b_1	−1.26	2.28	1.35	1.19	95	2614	3001	1.33	0.11
	b_2	−1.25	2.29	1.36	1.01	93	2476	3027	1.31	0.10
	b_3	−1.22	2.28	1.35	1.02	96	2613	2889	1.28	0.12
	b_4	−1.22	2.28	1.35	1.01	96	2610	2894	1.28	0.11
	b_5	−0.87	2.35	1.35	1.04	91	2535	2412	0.94	0.08
	b_6	−0.84	2.35	1.35	1.04	94	2608	2400	0.90	0.08
3	b_7	−1.25	2.28 × 3	1.35 × 3	1.01	96 × 3	2608	2988	1.28	0.38
					1.12 × 2		2614	1519		
							2610	1683		
	b_8	−1.21	2.28 × 2	1.35 × 3	1.02 × 2	95 × 2	2614 × 3	2890 × 3	1.25	0.36
			2.45		1.59	--				
	b_9	−1.21	2.28 × 3	1.35 × 3	1.02 × 3	96 × 3	2614 × 2	2890 × 2	1.27	0.36
							2615	2524		
	b_{10}	−1.12	2.28 × 3	1.36 × 3	1.01 × 3	103 × 3	2441 × 3	2957 × 3	0.93	0.29
	b_{11}	−0.82	2.33 × 2	1.35 × 2	1.02 × 2	96 × 2	2532	3153	1.02	0.23
			2.48	1.39	1.97	--	2579	2515		
							2328	--		
6	b_{12}	−1.27	2.28 × 6	1.35 × 6	1.01 × 6	96 × 6	2613 × 6	2981 × 6	1.34	0.74
	b_{13}	−1.11	2.37[c]	1.35 × 6	0.99[c]	96 × 6	--	--	1.10	0.66
			2.31 × 2[c]		1.02 × 2[c]					
			2.28 × 3		1.01 × 3					
	b_{14}	−1.09	2.28 × 5	1.35 × 6	1.01 × 5	94 × 5	--	--	1.26	0.71
			2.55		3.04	--				
	b_{15}	−1.06	2.30 × 3[c]	1.35 × 6	1.02 × 3[c]	98 × 3[c]	2612[c]	2729[c]	1.14	0.64
							2559[c]	2773[c]		
			2.28 × 3		1.01 × 3	97 × 3	2585[c]	2785[c]		
							2614 × 3	2906 × 3		
	b_{16}	−0.84	2.28 × 3	1.35 × 6	1.01 × 3	97 × 3	--	--	1.36	0.67
			2.55 × 3		2.95 × 3	--				

Binding energy (E_B); calculated distance between the Zn_S and S of SH ($d(Zn_S{-}SH_a)$); SH distance ($d(S{-}H)$); O_S surface atom and H distance ($d(O_S{-}H_b)$); bond angle between the Zn_S and SH ($\angle Zn_SSH$); calculated S−H stretch ($\nu(S{-}H_a)$) and O−H stretch ($\nu(O_S{-}H_b)$); band gap (E_g); charge transfer (Δq). [a]Calculated symmetric stretch of H_2S molecule. [b]Symmetric stretch of H_2O.[18] [c]H_2S adsorbed on the inside of the faceted-nanotube.

conduction band contributing to the reduced band gap (see Table 1). At these higher coverages, however, the impurity state at the top of the valence band increases in intensity until it is greater than that of the clean nanowire (see Figure 3b for structure a_5). This state is primarily due to mixing of the S 3p states with O 2p then Zn 3d orbitals. The impurity state at the bottom of the conduction band does not extend to as low energy for this structure, which results in a smaller decrease in the band gap at the higher gas coverages.

3.2. ZnO Faceted-Nanotube. *3.2.1. Binding Energy and Geometry.* On the faceted-nanotube, there were found to be 16 stable structures of adsorbed H_2S (Figure 4). The H_2S molecule again dissociated during geometry optimization to give adsorbed H and SH, as it did on the nanowire, which may be expected as both nanostructures have $(10\bar{1}0)$ surface facets on their sides. The larger number of structures found for this nanostructure can be attributed to the larger diameter of the faceted-nanotube (~16.59 Å) compared to the nanowire (~9.81 Å) which allows for a greater number of surface adsorption sites. Also, as the faceted-nanotube is hollow, we have shown that H_2S is able to adsorb on the inside of the faceted-nanotube. Furthermore, adsorption of H_2S on both the inside and outside at the same time is also possible at higher coverages. This may allow for greater use of faceted-nanotubes within nanosensors, as there are more adsorption sites available for gas detection within a corresponding area.

The BE and calculated geometries of these structures are presented in Table 2. H_2S preferentially adsorbs on the outside of the faceted-nanotube, having a stronger BE, and prefers to be located in the middle of the $(10\bar{1}0)$ surface facet, away from the edges of the nanostructure. This explains why adsorption on the nanowire was weaker, as each of the topmost surface Zn sites on the nanowire faces are equivalent to the sites on the edges of the faces on the faceted-nanotube.

It should be noted that the BE is stronger when the H and SH species both adsorb on the same facet (or edge) of the faceted-nanotube (e.g., structure b_1, BE = −1.25 eV) than when the H adsorbs on a different face to the SH species (e.g., structure b_5, BE = −0.87 eV). This difference may be due to the difference in the adsorbed bond lengths.

The calculated BE values for the H_2S/faceted-nanotube structures with similar adsorption geometries follow the same trend to those evaluated for the nanowire. Specifically, the most stable structures with 1 H_2S (b_1), 3 H_2S (b_7) and 6 H_2S (b_{12}) compared to those of the nanowire (a_1, a_3, and a_5 in Figure 2) only have BE values that differ by ≤0.05 eV.

The bond distances between the adsorbed H and SH species and the surface atoms on the faceted-nanotube are generally

dx.doi.org/10.1021/jp408916b | J. Phys. Chem. C 2013, 117, 26106−26118

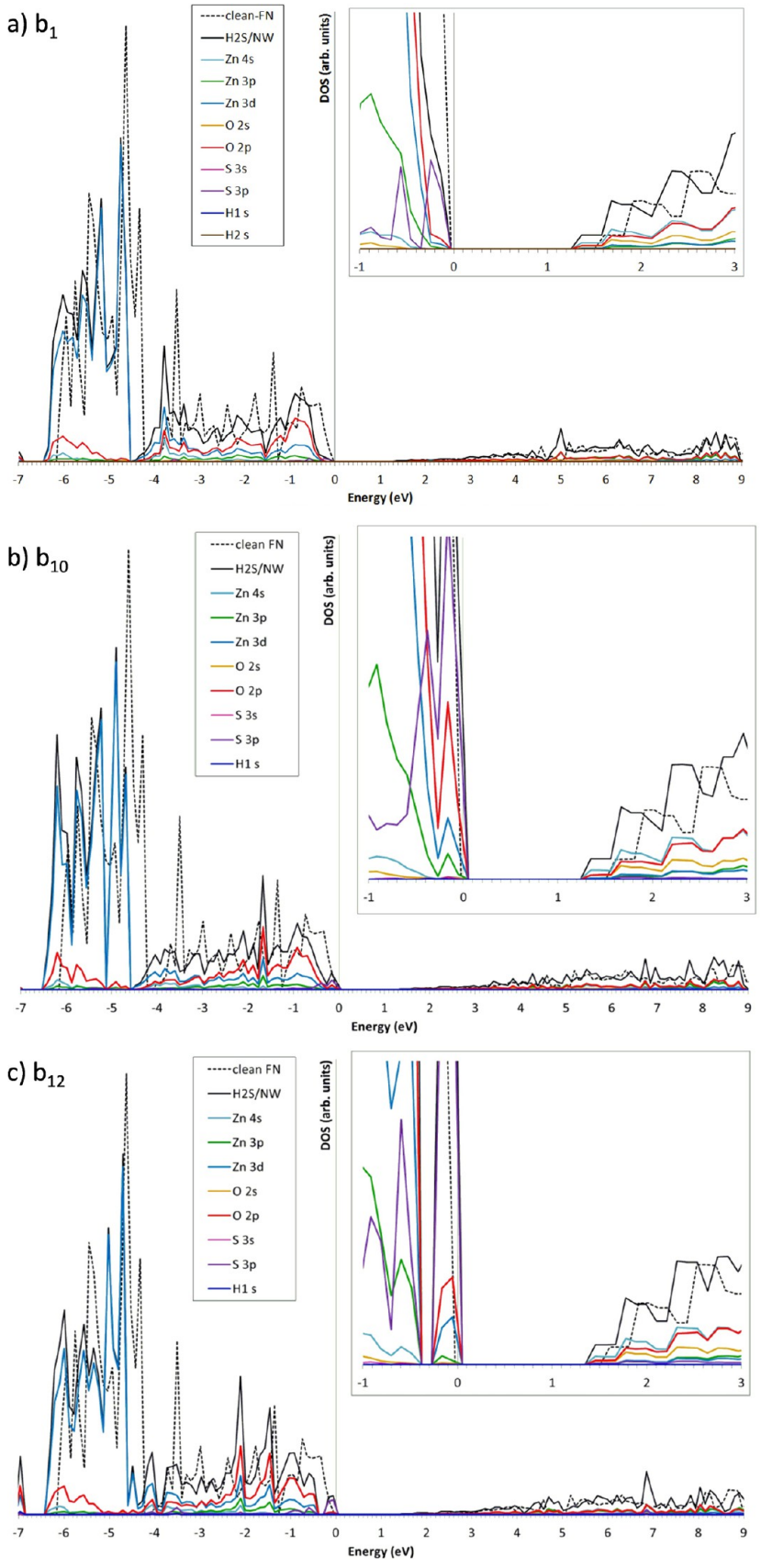

Figure 5. Density of states of H_2S adsorbed on the ZnO faceted-nanotube: (a) structure b_1, (b) structure b_{10}, and (c) structure b_{12}. Inset shows magnified region of DOS around the band gap.

dx.doi.org/10.1021/jp408916b | J. Phys. Chem. C 2013, 117, 26106−26118

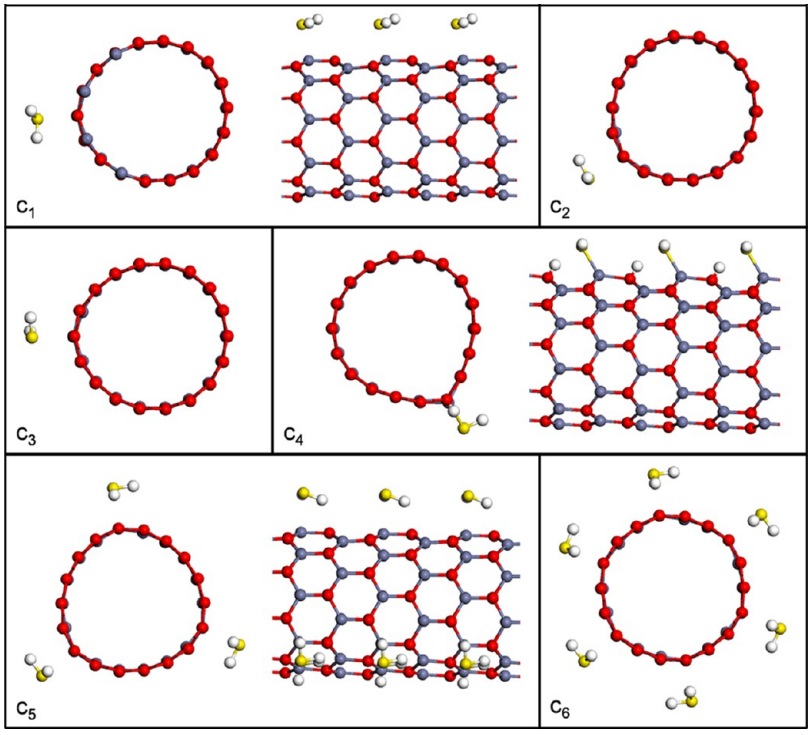

Figure 6. ZnO nanotube with one (c_{1-4}), three (c_5), or six (c_6) H_2S molecules adsorbed.

Table 3. Calculated Properties of H_2S Adsorbed on the ZnO Nanotube at the Coverages Indicated

#H_2S	structure	E_B (eV)	$d(Zn_S-SH_a)$ (Å)	$d(S-H_a)$ (Å)	$d(O_S-H_b)$ (Å)	$\nu(S-H_a)$ *Asy.* (cm^{-1})	$\nu(S-H_a)$ *Sy.* (cm^{-1})	$\nu(O_S-H_b)$ (cm^{-1})	E_g (eV)	Δq (e)
--	H_2S	--	--	1.35	--	2643[a]	2627[b]	3657[c]	--	--
--	ZnO	--	--	--	--	--	--	--	1.78	--
1	c_1	−0.24	2.68	1.35	3.31	2635	2620	--	1.79	0.09
	c_2	−0.24	2.69	1.35	2.86	2625	2611	--	1.78	0.09
	c_3	−0.23	2.67	1.35	3.42	2635	2619	--	1.77	0.09
	c_4	−0.67	2.31	1.35	1.01	2613	--	2955	1.74	0.09
3	c_5	−0.23	2.71 × 3	1.35	2.34 × 3	2624 × 3	2531 × 3	--	1.84	0.21
6	c_6	−0.22	2.76 × 6	1.35	2.18 × 6	2627 × 3	2466 × 6	--	1.91	0.31

Binding energy (E_B); calculated distance between the Zn_S and S of SH ($d(Zn_S-SH_a)$); SH distance ($d(S-H_a)$); O_S atom and H distance ($d(O_S-H_b)$); calculated S−H stretch ($\nu(S-H_a)$), S−H bend ($\nu(HSH)$) and O−H stretch ($\nu(O_S-H_b)$); band gap (E_g); charge transfer (Δq). [a]Calculated symmetric stretch. [b]Calculated asymmetric stretch of H_2S. [c]Symmetric stretch of H_2O.[18]

similar to those calculated for the nanowire consistent with the similar binding energies. The Zn_S−SH distance is slightly larger (2.35 Å) in certain structures (e.g., structure b_5), which indicates why they have a weaker binding energy. We also note that at the higher coverages we found some structures that are stable with a mixture of dissociatively and associatively adsorbed molecules (structures b_{11}, b_{16}). In structure b_{11}, one of the H_2S molecules remains intact when adsorbed on the inside of the faceted-nanotube, while the other two molecules dissociate. For structure b_{16}, three of the molecules dissociate while the other three adsorb associatively. These geometries give longer Zn−S bond lengths for the undissociated molecules of 2.48 Å (for b_{11}) and 2.55 Å (for b_{16}), which is as expected. Also, the BE values are weaker for these structures.

3.2.2. Vibrational Frequencies. The calculated vibrational frequencies of H_2S adsorbed on the faceted-nanotube were found to differ depending on the location of the H and SH species (see Table 2). When H_2S is adsorbed on the outside of the faceted-nanotube the S−H_a stretch for these structures (which varies from 2608 to 2618 cm^{-1}) is similar to the free H_2S molecule (2627 cm^{-1}) as well as those calculated for the H_2S/nanowire (2614−2616 cm^{-1}). However, there is a clear shift in the S−H_a stretch when H_2S adsorbs on the inside of the faceted-nanotube (by as much as 100 cm^{-1} to a lower frequency). This redshift may allow H_2S adsorbed on the inside of the faceted-nanotube to be distinguished experimentally from H_2S adsorbed on the outside of the structure. For the structures where H_2S is associatively adsorbed, as expected, there is no O−H stretch.

3.2.3. Charge Transfer, Band Structure, and Density of States. The calculated charge transfer (Δq) for the H_2S/faceted-nanotube structures (Table 2) are similar to those for the nanowire, again showing a positive charge transfer that increases as the gas coverage increases.

The calculated band gap of the clean faceted-nanotube (1.54 eV) agrees well with that calculated by Pan and Feng of 1.47 eV.[29] From the DOS (Figure 5), the top of the valence band is dominated by O 2p states, followed by Zn 3d states. The Zn 4s and O 2p and 2s orbitals contribute most to the bottom of the conduction band.

dx.doi.org/10.1021/jp408916b | J. Phys. Chem. C 2013, 117, 26106−26118

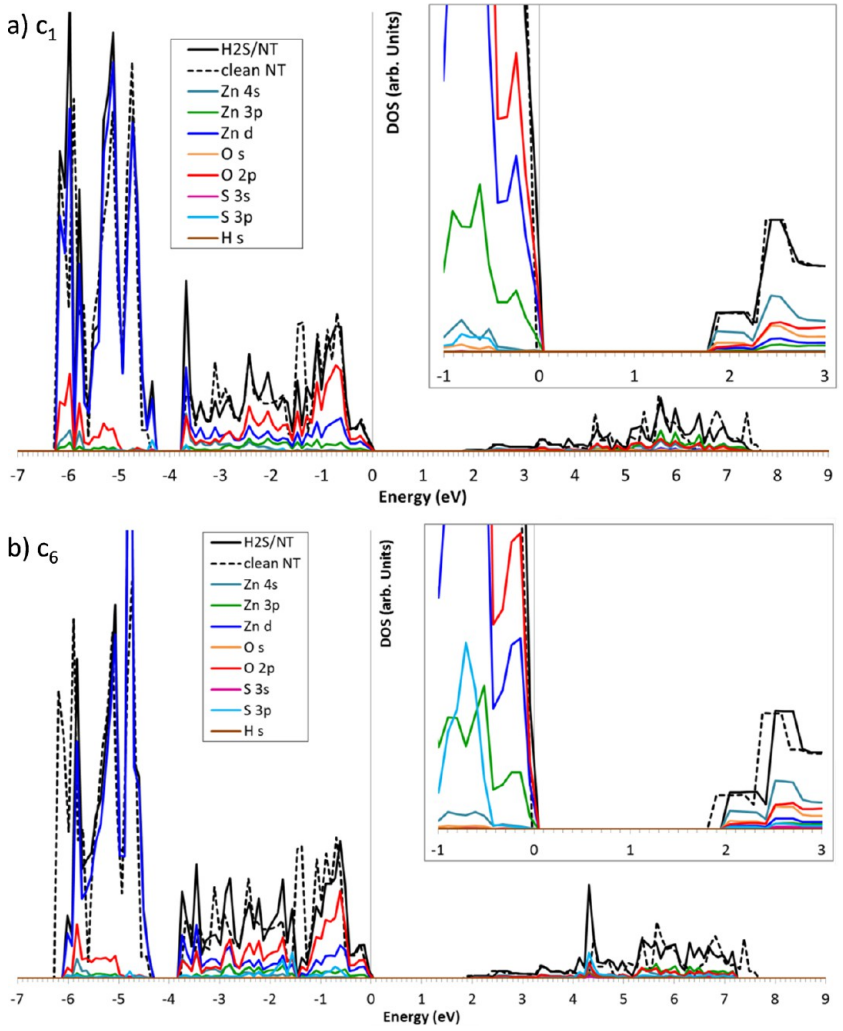

Figure 7. Density of states of H_2S adsorbed on the ZnO nanotube: (a) structure c_1 and (b) structure c_6. Inset shows magnified region of DOS around the band gap.

Table 4. Ab Initio MD Simulations Performed for H_2S Reacting with the Nanowire, Faceted-Nanotube, and Nanotube[a]

nanostructure	#H_2S	temp. (K)	simulation time (ps)	reaction
nanowire	1	300	2.5	$H_2S_{(g)} \rightarrow H_{(ads)} + SH_{(ads)}$
	3	300	5	$3H_2S_{(g)} \rightarrow 3H_{(ads)} + 3SH_{(ads)}$
		700	5	$3H_2S_{(g)} \rightarrow 3H_{(ads)} + 3SH_{(ads)}$
faceted-nanotube	1[b]	300	6.5	$H_2S_{(g)} \rightarrow H_{(ads)} + SH_{(ads)}$
	3	300	10.5	$3H_2S_{(g)} \rightarrow 3H_{(ads)} + 3SH_{(ads)}$
		700	3	$3H_2S_{(g)} \rightarrow H_2S_{(g)} + 2H_{(ads)} + 2SH_{(ads)}$
nanotube	1	700	15	$H_2S_{(g)} \rightarrow H_{(ads)} + SH_{(ads)}$
	6	700	3.5	$6H_2S_{(g)} \rightarrow 3H_2S_{(g)} + 3H_{(ads)} + 3SH_{(ads)} \rightarrow$ Nanotube collapse

[a]The simulation temperature, time and surface reaction are indicated. [b]In this simulation H_2S was placed on the inside of the nanostructure.

After adsorption of H_2S, the size of the band gap decreases (Table 2), irrespective of the gas coverage. For the most stable structure with 1, 3, or 6 adsorbed H_2S molecules, the band gap is reduced by ~0.2 eV, which is similar to adsorption of H_2S on the nanowire (−1.28 to −1.45 eV). Interestingly, a greater decrease in the band gap was calculated when H_2S adsorbs on the inside of the faceted-nanotube (0.93 - 0.94 eV). We suggest this is due to the closer proximity of the adsorbed H_2S, H or SH species and their interaction with each other.

We present the DOS for three representative structures: structure b_1, where 1 H_2S molecule is adsorbed on the outside; structure b_{10}, where 3 H_2S molecules are adsorbed on the inside; and structure b_{12}, where 6 H_2S molecules are adsorbed on the outside of the faceted-nanotube. The DOS of structure b_1 (Figure 5a) shows a shift of the conduction band to lower energy, which gives rise to the decrease in the band gap. Similar to the NW, an impurity state due to mixing of the S 2p orbitals with the Zn and O orbitals is found at the bottom of the conduction band. While the intensity of the states at the top of the valence band is reduced, the major contribution is from the S 2p orbital. For structure b10, there is again a shift to lower energy of the bottom of the conduction band due to an impurity state from mixing of the S 2p and the Zn and O orbitals. At this higher coverage, the intensity of the impurity state at the top of the valence band is greater than at the lower gas coverage. This impurity state extends above the level of the clean faceted-nanotube DOS. For structure b_{12}, where six H_2S molecules are adsorbed, the same change to the conduction band is seen, but the intensity of the impurity states above the

dx.doi.org/10.1021/jp408916b | J. Phys. Chem. C 2013, 117, 26106−26118

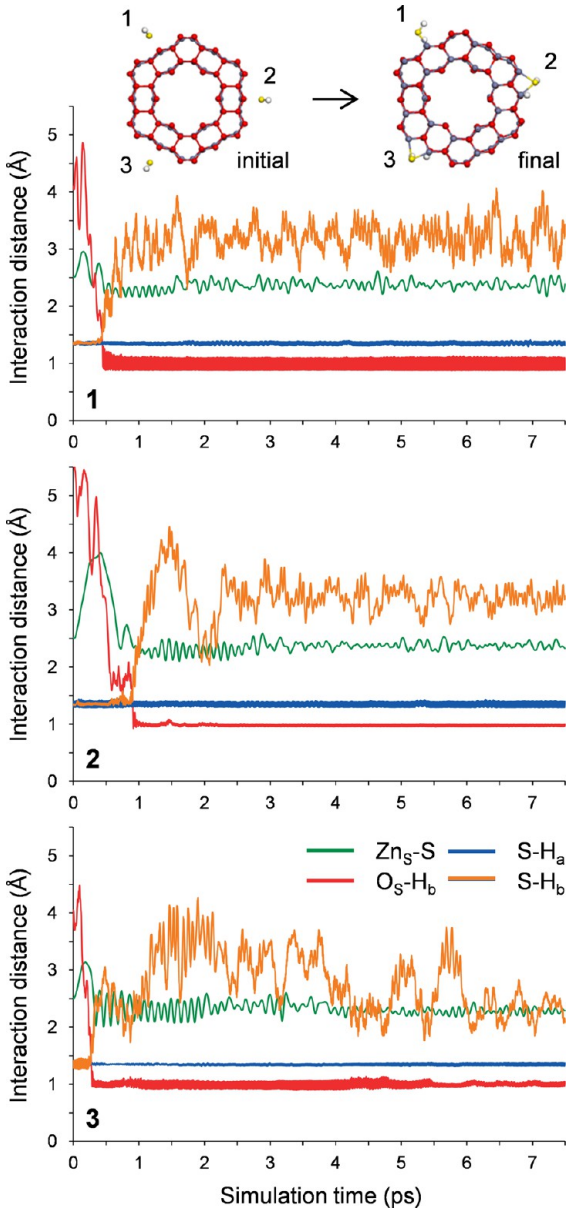

Figure 8. Interaction distances between specific pairs of atoms during the AIMD simulation of H_2S adsorbing on the faceted nanotube at 300 K.

top of the valence band has increased further and shifted further above the clean DOS level.

3.3. ZnO Nanotube. *3.3.1. Binding Energy and Geometry.* As can be seen from Figure 6, H_2S does not dissociate on the nanotube, but adsorbs molecularly. This is consistent with the BE values (Table 3), which are significantly weaker (all below −0.25 eV) than on the nanowire and faceted-nanotube, indicating physiorption. The distance between the S atom and the closest surface Zn atom (~2.7 Å) is also larger than for dissociative adsorption on the nanowire and faceted-nanotube (~2.3 Å), which is again consistent with weak bonding. It can be seen for all structures (Figure 6), however, that H_2S partly distorts the nanotube structure, whereas this was not the case for the nanowire and faceted-nanotube, which have thicker walls. It is important to note that the weaker BE for the nanotube indicates H_2S may be more easily removed from the surface via heating, allowing the nanotube to recover more readily in a gas sensor context than the other nanostructures investigated.

In order to determine whether a dissociated H_2S molecule is stable on the nanotube, we started the calculation with an adsorbed H and SH species on the surface of the nanotube and performed a geometry optimization. The optimized structure is shown as structure c_4 in Figure 6, and it can be seen that H_2S remains dissociated, giving a stronger binding energy of −0.67 eV than the physisorbed structure. While the binding is weaker than on either the nanowire or the faceted-nanotube, this indicates that there is a barrier to partial dissociation on the nanotube that is essentially zero on the other nanostructures.

Overall, our calculations show that the nanostructure morphology does have an effect on the reaction of H_2S.

3.3.2. Vibrational Frequencies. The calculated vibrational frequencies for H_2S adsorbed on the nanotube are listed in Table 3. As the H_2S is molecularly adsorbed, the asymmetric stretch, symmetric stretch, and bend values are calculated. The asymmetric stretch for each structure (~2635 cm^{-1}) is similar to the free H_2S molecule (2643 cm^{-1}) differing by less than 10 cm^{-1}. The symmetric stretch is also similar to the free molecule, however, it is shifted to a lower frequency (red-shifted) with the size of the shift increasing for a higher gas coverage. This indicates that there is some interaction between adjacent H_2S molecules. Hence, one could use experimental techniques to distinguish whether H_2S was adsorbed molecularly or dissociatively on the nanostructure.

3.3.3. Charge Transfer, Band Structure, and Density of States. The calculated charge transfer values for these structures (Table 3) were smaller than on the other nanostructures, consistent with the weaker binding. The calculated band gap was also determined to remain largely unaltered by the adsorption of H_2S (Table 3), changing by ≤0.13 eV. However, there is a calculated transfer of charge from H_2S to the nanotube, hence we suggest that these nanostructures may still detect H_2S.

For structure c_1 (Figure 7a), the presence of adsorbed H_2S leads to an increase in intensity of states at −2 eV, −3.7 eV, and −4.4 eV, however, there is little change to the states at the top of the valence band or bottom of the conduction band, which due to the weak binding results in essentially no change to the band gap. For structure c6 (Figure 7b), the H_2S contributes more strongly to states from approximately −0.7 eV to −0.45 eV below the top of the valence band due to their higher coverage on the surface. The greater concentration of H_2S also results in a shift to higher energy of ~0.15 eV of the bottom of the conduction band, which results in the small increase of 0.13 eV in the band gap. Overall, the changes to the electronic structure are not as significant on this nanostructure due to the weaker binding.

3.4. Effect of Temperature on the H_2S Reaction. Ab initio molecular dynamics (AIMD) simulations were performed for H_2S reacting with the nanowire, faceted-nanotube and nanotube, under the conditions shown in Table 4. For each simulation, H_2S was placed ~3 Å from the surface and allowed to freely move in all directions at a simulation temperature of 300 K and/or 700 K. These two temperatures were chosen as they cover the operating temperatures used for detection of H_2S with ZnO nanosensors (for example, refs 5, 7, and 30−32).

From Table 4 one can see that the surface reactions occurring on the nanowire and faceted-nanotube at 300 K are identical, with H_2S dissociatively adsorbing on the nanostruc-

dx.doi.org/10.1021/jp408916b | J. Phys. Chem. C 2013, 117, 26106−26118

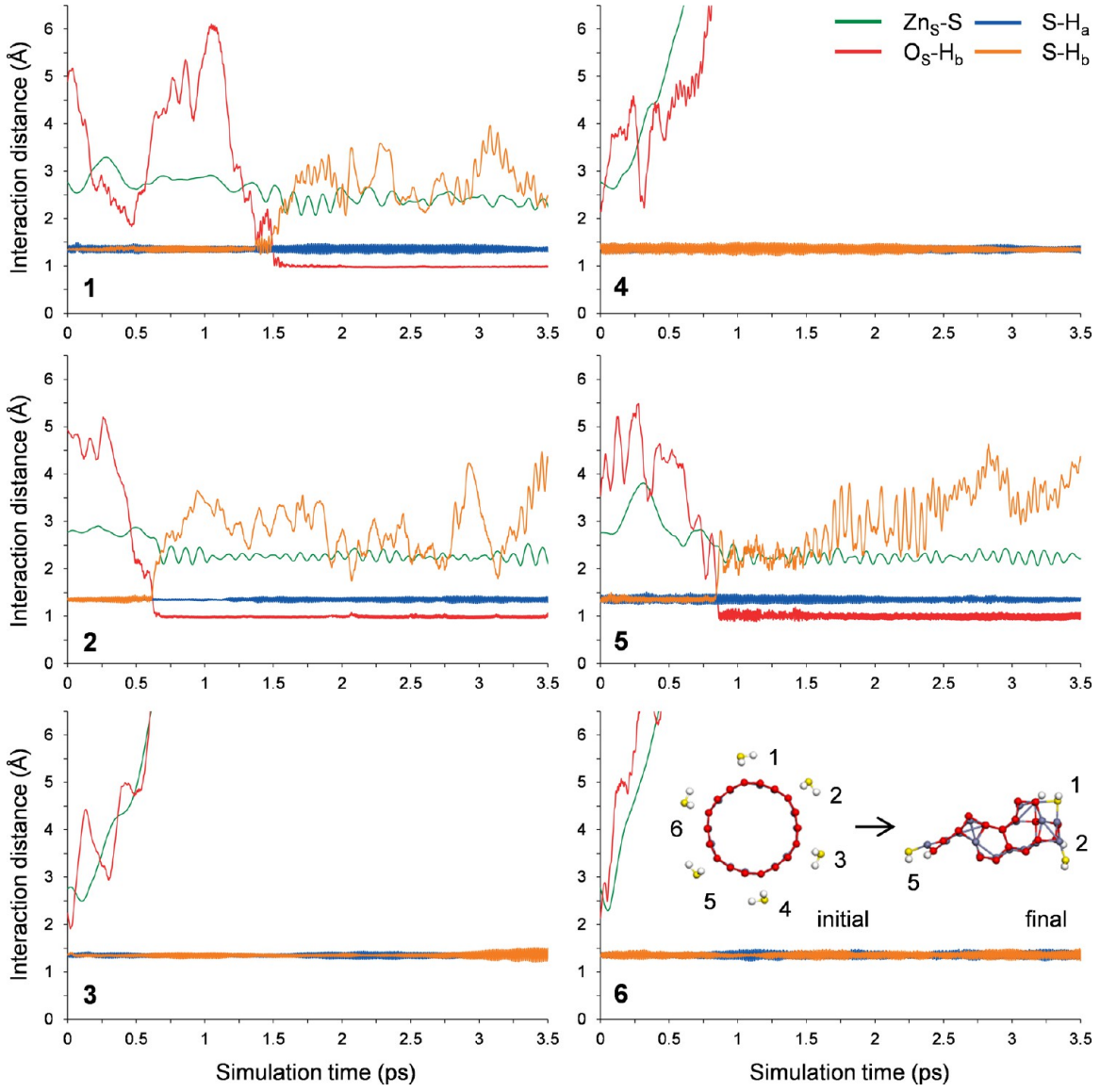

Figure 9. Interaction distances between specific pairs of atoms during the AIMD simulation of 6 H_2S molecules reacting with the nanotube.

Table 5. Ab Initio Molecular Dynamics Simulations for H_2S Adsorbed on the Nanowire, Faceted-Nanotube, and Nanowire[a]

nanostructure	#H_2S	structure[b]	temp. (K)	time (ps)
nanowire	--	--	--	--
faceted-nanotube	1	a_1	300	1.5
	1	a_5		1
	3	b_1		2
	6	c_1		1
	1	a_1	700	1.5
	1	a_2		10.5
nanotube	1	a_4	700	5

[a]Each simulation was performed starting from the structure obtained after geometry optimization. [b]Structures that were used as the starting geometry of the simulation can be found in Figures 2, 4, and 6.

ture to form adsorbed H and SH, as was seen after the geometry optimization.

These surface reactions can be analyzed further by looking at the interaction distances between the adsorbate and the nanostructure surface during the simulation (as shown in Figure 8 for three H_2S molecules reacting with the faceted-nanotube at 300 K). Each H_2S molecule is shown separately for distinction, with the distance between pairs of atoms plotted as a function of time. It can be seen that each H_2S molecule was initially placed ~2.5 Å away from the faceted-nanotube surface (as indicated by the initial distance between the S atom of H_2S and the closest Zn atom of the nanowire). As the simulation progresses there are fluctuations in the S−H distances, which are attributed to the expected vibration of these bonds at 300 K. The Zn_S−S distances are then found to decrease while the S−H_b distances increase, as seen at ~0.25, 0.5, and 1 ps for molecule 3, 1 and 2, respectively. This indicates that the H_2S molecule is oscillating closer to the faceted-nanotube surface until the S−H_b bond breaks and SH species adsorbs to a surface Zn atom (Zn_S). At the same time the O_S−H_b distance decreases indicating that the H_b atom adsorbs to a surface oxygen (O_S) atom. The S−H_a distance remains constant (except for the expected bond vibrations) for the length of the simulation which indicates that the SH species remains intact. For the remainder of the simulation (up to ~6 ps) the

dx.doi.org/10.1021/jp408916b | J. Phys. Chem. C 2013, 117, 26106−26118

interaction distances remain fairly constant indicating that the structure is stable with this adsorbed configuration.

For the reaction of H_2S with the faceted-nanotube at the higher temperature (700 K), it was found that two H_2S molecules dissociatively adsorbed on the surface as SH and H, while the third H_2S molecule moved away from the surface (see Table 4). This could be caused by the increased vibrations that occur at elevated temperatures, overcoming any barrier to desorption. We note that complete dissociation may be possible during a longer simulation time, however, our results show that there is a higher barrier to dissociation of the second S−H bond, consistent with the results of Ling et al.,[9] who determined this barrier to be 51.47 kJ mol^{-1} for dissociation on the $(10\bar{1}0)$ planar surface.

For the nanotube, performing the simulation at 700 K resulted in H_2S dissociatively adsorbing on the surface as H and SH. This is in contrast to the geometry optimization calculation where H_2S physisorbed molecularly, but confirming that the elevated temperature provides additional energy into the system to overcome the barrier to dissociation.

For a higher concentration of H_2S, we found that the nanotube was unstable. The distance between pairs of atoms during the simulation with 6 H_2S molecules is shown in Figure 9. At this higher simulation temperature somewhat larger vibrations (as expected) of the S−H bonds occur. After ∼0.5, 0.75, and 1.5 ps it can be seen that H_2S molecules labeled 2, 5 and 1, respectively, dissociatively adsorb on the surface. After a similar time, molecules 3, 4, and 6 desorb from the surface as indicated by the large increase in the Zn_S-S and O_S-H_b distances. After a further ∼2 ps of simulation time, however, the nanotube structure collapses, as shown by the large fluctuation of the SH species distances and also from the geometry of the final structure shown in Figure 9 (inset). We confirmed that it is the presence of H_2S that causes this instability, as an MD simulation of the clean nanotube shows that its structure remains intact.

A number of the other optimized structures (shown in Figures 2, 4, and 6) were also analyzed using AIMD (see Table 5). In all cases it was found that the H_2S/nanostructure systems remained stable for the length of the simulations, with the H and SH species remaining adsorbed to the surface. It is interesting to note that during these simulations the adsorbed S and SH species did not recombine and desorb from the nanostructure, which one might expect to be important for the use of these nanostructures as gas sensors. One reason we may not see this reaction is that the simulations may need to be run for longer, or that not all possible pathways were analyzed during the simulation. It should be noted, however, that such a reaction may also not be thermodynamically favorable as it is known that ZnO can be converted to ZnS using H_2S.[33] our further work will examine the effect of defects and preadsorbed species on the reaction of H_2S with ZnO nanostructures.

4. CONCLUSIONS

Using density functional theory calculations it was determined that H_2S dissociatively adsorbs on both the ZnO nanowire and faceted-nanotube but adsorbs molecularly on the nanotube. H_2S is able to adsorb in multiple locations on each of the nanostructures, which is necessary for an effective gas sensor. The greater number of stable structures for the faceted-nanotube compared to the nanowire is due to the fact that H_2S can adsorb on the inside of the faceted-nanotube, and also because the faceted-nanotube has a larger surface area. This may allow greater use of faceted-nanotubes for sensing as there are more adsorption sites available for gas detection. For all nanostructures, H_2S behaves as a charge donor, with charge being transferred from H_2S to the nanostructure. When H_2S interacts with the nanostructure surface the band gap decreases for the nanowire and faceted-nanotube, while the band gap is only slightly changed for the nanotube, consistent with the weak binding. Ab initio molecular dynamics simulations indicate that at elevated temperatures dissociation of H_2S on the nanotube is facilitated as the barrier to dissociation is overcome, however, recombination and desorption of H_2S does not occur within the simulation time. This indicates that H_2S may poison the surface, preventing further molecules from reacting with the nanostructure surface and being detected. Our future work will determine the effect of surface defects and preadsorbed oxygen on the H_2S-nanostructure reactions.

Overall, we have shown that the gas-nanostructure reaction of H_2S is influenced by the ZnO nanostructure morphology, as well as the gas coverage and reaction temperature. This information provides details about the gas sensing mechanism of H_2S with ZnO nanostructures to assist in their further development.

AUTHOR INFORMATION

Corresponding Author

*E-mail: michelle.spencer@rmit.edu.au. Current address: School of Applied Sciences, RMIT University, GPO Box 2476, Melbourne, Victoria 3001, Australia. Phone: +613 9925 9697.

Notes

The authors declare no competing financial interest.

ACKNOWLEDGMENTS

Computational facilities are gratefully acknowledged from the following facilities: NCI National Facility systems at the Australian National University through the National Computational Merit Allocation Scheme supported by the Australian Government, VPAC, MASSIVE, IVEC, and Hercules (at La Trobe). A La Trobe University eResearch grant is gratefully acknowledged (M.J.S.S.). We thank James McCallum for running some of the optimized structures of H_2S adsorbed on the nanowire and (9,0) nanotube.

REFERENCES

(1) Reiffenstein, R. J.; Hulbert, W. C.; Roth, S. H. Toxicology of Hydrogen-Sulfide. *Annu. Rev. Pharmacol. Toxicol.* **1992**, *32*, 109−134.
(2) Hendrickson, R. G.; Chang, A.; Hamilton, R. J. Co-worker Fatalities from Hydrogen Sulfide. *Am. J. Ind. Med.* **2004**, *45*, 346−350.
(3) Kourtidis, K.; Kelesis, A.; Petrakakis, M. Hydrogen sulfide (H_2S) in urban ambient air. *Atmos. Environ.* **2008**, *42*, 7476−7482.
(4) Klingshirn, C. ZnO: From Basics Towards Applications. *Phys. Status Solidi B* **2007**, *244*, 3027−3073.
(5) Cao, Y.; Jia, D.; Wang, R.; Luo, J. Rapid One-Step Room-Temperature Solid-State Synthesis and Formation Mechanism of Zno Nanorods as H_2S-Sensing Materials. *Solid-State Electron.* **2013**, *82*, 67−71.
(6) Wang, C.; Chu, X.; Wu, M. Detection of H_2S Down to ppb Levels at Room Temperature Using Sensors Based on ZnO Nanorods. *Sens. Actuators, B* **2006**, *113*, 320−323.
(7) Kim, J.; Yong, K. Mechanism Study of ZnO Nanorod-Bundle Sensors for H_2S Gas Sensing. *J. Phys. Chem. C* **2011**, *115*, 7218−7224.
(8) Casarin, M.; Maccato, C.; Vittadini, A. An LCAO-LDF Study of the Chemisorption of H_2O and H_2S on ZnO(0001) and ZnO$(10\bar{1}0)$. *Surf. Sci.* **1997**, *377*, 587−591.

(9) Ling, L.; Zhang, R.; Han, P.; Wang, B. DFT Study on the Sulfurization Mechanism during the Desulfurization of H_2S on the ZnO Desulfurizer. *Fuel Process. Technol.* **2013**, *106*, 222−230.
(10) Goclon, J.; Meyer, B. The Interaction of H_2S with the ZnO(1010) Surface. *Phys. Chem. Chem. Phys.* **2013**, *15*, 8373−8382.
(11) Kresse, G.; Furthmuller, J. Efficiency of Ab-Initio Total Energy Calculations for Metals and Semiconductors Using a Plane-Wave Basis Set. *Comput. Mater. Sci.* **1996**, *6*, 15−50.
(12) Kresse, G.; Furthmuller, J. Efficient Iterative Schemes for Ab Initio Total-Energy Calculations Using a Plane-Wave Basis Set. *Phys. Rev. B* **1996**, *54*, 11169−11186.
(13) Kresse, G.; Hafner, J. Ab-Initio Molecular-Dynamics for Open-Shell Transition-Metals. *Phys. Rev. B* **1993**, *48*, 13115−13118.
(14) Perdew, J. P.; Wang, Y. Accurate and Simple Analytic Representation of the Electron-Gas Correlation-Energy. *Phys. Rev. B* **1992**, *45*, 13244−13249.
(15) Vanderbilt, D. Soft Self-Consistent Pseudopotentials in a Generalized Eigenvalue Formalism. *Phys. Rev. B* **1990**, *41*, 7892−7895.
(16) Monkhorst, H. J.; Pack, J. D. Special Points for Brillouin-Zone Integrations. *Phys. Rev. B* **1976**, *13*, 5188−5192.
(17) Spencer, M. J. S.; Wong, K. W. J.; Yarovsky, I. Density Functional Theory Modelling of ZnO(1010) and ZnO(2110) Surfaces: Structure, Properties and Adsorption of N_2O. *Mater. Chem. Phys.* **2010**, *119*, 505−514.
(18) Lide, D. R., *CRC Handbook of Chemistry and Physics*, 94th ed.; Taylor and Francis: Boca Raton, FL, 2013−2014; http://www.hbcpnetbase.com, accessed online July 2013.
(19) Henkelman, G.; Arnaldsson, A.; Jonsson, H. A Fast and Robust Algorithm for Bader Decomposition of Charge Density. *Comput. Mater. Sci.* **2006**, *36*, 354−360.
(20) Blochl, P. E. Projector augmented-wave method. *Phys. Rev. B* **1994**, *50*, 17953−17979.
(21) Nose, S. A Unified Formulation of the Constant Temperature Molecular-Dynamics Methods. *J. Chem. Phys.* **1984**, *81*, 511−519.
(22) Lin, J.; May, J. A.; Didziulis, S. V.; Solomon, E. I. Variable-Energy Photoelectron Spectroscopic Studies of Hydrogen Sulfide Chemisorption on Cuprous Oxide and Zinc Oxide Single-Crystal Surfaces: HS- Bonding to Copper(I) and Zinc(II) Sites Related to Catalytic Poisoning. *J. Am. Chem. Soc.* **1992**, *114*, 4718−4727.
(23) Spencer, M. J. S.; Yarovsky, I.; Wlodarski, W.; Kalantar-zadeh, K. In *Density Functional Theory Study of ZnO Nanostructures for NO and NO_2 Sensing*; Proceedings of Transducers and Eurosensors '07, Lyon, France, June 10−14; IEEE: Lyon, France, 2007; pp 987−990.
(24) Spencer, M. J. S.; Yarovsky, I. ZnO Nanostructures for Gas Sensing: Interaction of NO_2, NO, O, and N with the ZnO(1010) Surface. *J. Phys. Chem. C* **2010**, *114*, 10881−10893.
(25) Spencer, M. J. S., Density Functional Theory Modeling of ZnO for Gas Sensor Applications. In *Chemical Sensors, Vol. 1, Series II*; Korotcenkov, G., Ed. Momentum Press: New York, 2012; Vol. *I*.
(26) Breedon, M.; Spencer, M. J. S.; Yarovsky, I. Adsorption of NO_2 on Oxygen Deficient ZnO($2\bar{1}\bar{1}0$) for Gas Sensing Applications: A DFT Study. *J. Phys. Chem. C* **2010**, *114*, 16603−16610.
(27) Breedon, M.; Spencer, M. J. S.; Yarovsky, I. Adsorption of NO and NO_2 on the ZnO(2110) Surface: a DFT Study. *Surf. Sci.* **2009**, *603*, 3389−3399.
(28) Spencer, M. J. S. Gas sensing Applications of 1D-nanostructured Zinc Oxide: Insights from Density Functional Theory Calculations. *Prog. Mater. Sci.* **2012**, *57*, 437−486.
(29) Pan, H.; Feng, Y. P. Semiconductor Nanowires and Nanotubes: Effects of Size and Surface-to-Volume Ratio. *ACS Nano* **2008**, *2*, 2410−2414.
(30) Liao, L.; Lu, H. B.; Li, J. C.; He, H.; Wang, D. F.; Fu, D. J.; Liu, C.; Zhang, W. F. Size Dependence of Gas Sensitivity of ZnO Nanorods. *J. Phys. Chem. C* **2007**, *111*, 1900−1903.
(31) Shinde, S. D.; Patil, G. E.; Kajale, D. D.; Gaikwad, V. B.; Jain, G. H. Synthesis of ZnO Nanorods by spray Pyrolysis for H_2S Gas Sensor. *J. Alloys Compd.* **2012**, *528*, 109−114.
(32) Zhang, N.; Yu, K.; Li, Q.; Zhu, Z. Q.; Wan, Q. Room-Temperature High-Sensitivity of H_2S Gas Sensor Based on Dendritic ZnO Nanostructures with Macroscale in Appearance. *J. Appl. Phys.* **2008**, *103*, 104305−104306.
(33) Dloczik, L.; Engelhardt, R.; Ernst, K.; Fiechter, S.; Sieber, I.; Konenkamp, R. Hexagonal nanotubes of ZnS by Chemical Conversion of Monocrystalline ZnO Columns. *Appl. Phys. Lett.* **2001**, *78*, 3687−3689.